ORIGINAL CONTRIBUTION

Paulo H. P. Macaúbas
Nicole R. Demarquette
John M. Dealy

Nonlinear viscoelasticity of PP/PS/SEBS blends

P. H. P. Macaúbas
N. R. Demarquette (✉)
Metallurgical and Materials Engineering
Department, Escola Politécnica,
São Paulo University,
Av. Prof. Mello Moraes 2463,
CEP 05508-900 São Paulo, SP, Brazil
E-mail: nick@usp.br

J. M. Dealy
Chemical Engineering Department,
McGill University, 3610 University Street,
Montreal, QC, H3A 2B2, Canada

Present address: P. H. P. Macaúbas
Department of Polymer Science
and Engineering,
Kyoto Institute of Technology,
606-8585 Sakyo-Ku, Matsugasaki, Kyoto,
Japan

Abstract The nonlinear viscoelastic behavior of polypropylene/polystyrene (PP/PS) blends compatibilized or not with the linear triblock co-polymer (styrene-ethylene-/butylene-styrene, SEBS) was investigated. Start-up of steady-shear at rates from 0.1 to 10 s^{-1} was carried out using a controlled strain rotational rheometer and a sliding plate rheometer for strain histories involving one or several shear rates. The shear stress and first normal shear stress difference were measured as functions of time, and the morphologies of the samples before and after shearing were determined. For each strain history except that involving a single shear rate of 0.1 s^{-1} the blends showed typical non-linear viscoelastic behavior: a shear stress overshoot/undershoot, depending on the history, followed by a steady state for each step. The first normal stress difference increased monotonically to a steady-state value. The values of the stresses increased with the addition of SEBS. The shear stress overshoot and undershoot and the times at which they occurred depended strongly on the strain history, decreasing for a subsequent shear rate step performed in the same direction as the former, and the time at which stress undershoot occurred increased for a subsequent shear rate step performed in the opposite direction, irrespective of the magnitude of the shear rate. This behavior was observed for all the blends studied. The time of overshoot in a single-step shear rate experiment is inversely proportional to the shear rate, and the steady-state value of N_1 scaled linearly with shear rate, whereas the steady-state shear stress did not. The average diameter of the dispersed phase decreased for all strain histories when the blend was not compatibilized. When the blend was compatibilized, the average diameter of the dispersed phase changed only during the stronger flows. Experimental data were compared with the predictions of a model formulated using ideas of Doi and Ohta (1991), Lacroix et al. (1998) and Bousmina et al. (2001). The model correctly predicted the behavior of the uncompatibilized blends for single-step shear rates but not that of the compatibilized blends, nor did it predict morphologies after shearing.

Keywords Nonlinear viscoelasticity · Polymer blends · Doi and Ohta Theory · Flow-induced morphology

Introduction

Due to their useful properties, polymer blends have many applications, including automotive, packaging, and aerospace. The properties of such blends depend strongly on morphology, as polymer blends of industrial interest are generally immiscible. However, the mechanisms that govern morphology development during processing are not well understood at present. Knowledge of the relationships between flow conditions and morphology would be very useful for the optimization of blend properties as well as for the development of models for processes such as the coalescence and breakup of the dispersed phase. Theoretical models have been developed that relate the development of morphology under flow to rheological properties (Doi and Ohta 1991; Lee and Park 1994; Lacroix et al. 1998; Maffetone and Minale 1998; Almusallam et al. 2000; Grmela et al. 2001; Bousmina et al. 2001; Jackson and Tucker 2003; Yu and Bousmina 2003).

In their pioneer work, Doi and Ohta (1991) predicted the rheological behavior and morphology evolution of a polymer blend during deformation. They considered a blend in which the components are Newtonian and have equal viscosities, densities and volume fractions. Their model predicts the behavior of such a blend in a homogenous flow using the concept of averaged interface orientation (q_{ij}) and total surface area per unit volume (Q), which quantify the morphology evolution during flow and were introduced by Batchelor (1970) and Onuki (1987). The Doi-Ohta model gives the following prediction of the components of the total stress tensor:

$$\sigma_{ij} = \eta_o(\kappa_{ij} + \kappa_{ji}) - \alpha q_{ij} - P\delta_{ij} \tag{1}$$

$$q_{ij} = \frac{1}{V}\int\left(n_i n_j - \frac{1}{3}\delta_{ij}\right)dS \tag{2}$$

where σ_{ij} = stress tensor, κ_{ij} = macroscopic velocity gradient tensor, q_{ij} = interface tensor, δ_{ij} = the Kronecker delta, α = interfacial tension, η_o = viscosity, P = isotropic pressure, V = volume, and n_i = components of the unit normal vector to a surface element dS of the volume V.

The Doi-Ohta theory also yields scaling laws for the shear stress and first normal stress difference for transient and steady flow regimes. Such scaling laws arise from the assumption in the Doi-Ohta model that considered the system is characterized by the interfacial tension and viscosity, but not by a temporal quantity. The predicted scaling law is that if a velocity gradient tensor $\kappa_{ij}(t)$ generates a stress tensor $\sigma_{ij}(t,\kappa_{ij}(t))$, then a new velocity gradient tensor of the form $c\kappa_{ij}(ct)$ generates a stress tensor c times larger than the stress at time ct under the velocity gradient $\kappa_{ij}(t)$, where c is a constant. This scaling law can be written as follows:

$$\sigma_{ij}(t, c_{ij}(ct)) = c\sigma_{ij}(ct,_{ij}(t)) \tag{3}$$

For steady-shear Eq. (3) reduces to

$$\sigma_{ij}(c\dot{\gamma}) = c\sigma_{ij}(\dot{\gamma}) \tag{4}$$

Experimentally determined scaling laws for the steady regime have been reported by several authors: Takahashi et al. (1994a) proposed scaling relations for mixtures closely obeying the conditions of the Doi-Ohta model: i.e. Newtonian liquids having very similar densities and viscosities. They also tested the Doi-Ohta model by varying the composition of the mixture and observed that both the shear stress and first normal stress difference were proportional to the shear rate. Guenther and Baird (1996) evaluated the Doi-Ohta theory using a blend of viscoelastic polymers whose viscosity curves were close together. They found that the first normal stress difference scaled linearly with the shear rate, considering both the contribution of interface and the total stress. Vinckier et al. (1996) tested the Doi-Ohta theory for immiscible blends of poly(isobutene) and poly(dimethylsiloxane) (PIB/PMDS) in which the viscosity ratios ranged from 0.15 to 6.6. This work was actually an extension of that of Takahashi et al. (1994b), who found that the simple scaling relations held for viscoelastic blends of equal viscosity but a wide range of volume fractions, provided that only the contribution of the interface was taken into account. Vinckier et al. (1996) found that the Doi-Ohta scalings hold only when only the interface contribution is taken into account, the shear rate does not exceed a critical value, and the viscosity ratio does not exceed four. Iza et al. (2001) reported that the linear scaling law between shear stress and shear rate was valid for blends of polystyrene and high-density polyethylene (PS/HDPE) whether or not compatibilized with the triblock copolymer SEBS or a specially synthesized block copolymer based on hydrogenated poly(butadiene) and polystyrene blocks (called MCL by the authors). However, for the same systems, significant deviations from Doi-Ohta theory for the first normal stress difference were observed. Scaling laws different from those of Doi and Ohta have been proposed on the basis of recent nonlinear viscoelastic models (Grmela et al. 2001; Yu et al. 2002; Jackson and Tucker 2003; Yu and Bousmina 2003).

In order to cope with a mismatch of component viscosities, Lee and Park (1994) proposed a new a mixing rule and additional terms in the Doi-Ohta expression for the total stress. Their mixing rule was later refined by Lacroix et al. (1998), who did not make use of the Cox-Merz rule. This mixing rule is given by Eqs. (5) and (6):

$$\sigma_{ij}^{bulk} = \eta_m\dot{\gamma}_{ij}\left(\frac{1 + 1.5H}{1 - H}\right) \tag{5}$$

$$H = \phi \frac{2(\eta_d - \eta_m)}{2\eta_d + 3\eta_m} \qquad (6)$$

where η_m = viscosity of the matrix, η_d = viscosity of the dispersed phase, ϕ = volume fraction of the dispersed phase, $\dot{\gamma}_{ij}$ = shear rate tensor. This mixing rule has been employed to make qualitative predictions of changes in morphology during shear flow (Lacroix et al. 1999).

Recently, Bousmina et al. (2001) improved the Doi-Ohta model by modifying the contribution of the interface, introducing a set of differential equations correlating the morphology evolution to breakup and coalescence phenomena:

$$\sigma_{ij}^{\text{interface}} = \alpha q_{ij} + 2C_2\left(\frac{2}{3}Q + 2q_{kj} - \frac{q_{ml}^2}{Q}\right)q_{ji} \qquad (7)$$

$$\frac{\partial q_{ij}(t)}{\partial t} = -q_{kj}\kappa_{ik} - q_{ki}\kappa_{jk} + \frac{2}{3}\delta_{ij}q_{lk}\kappa_{lk} - \frac{Q}{3}(\kappa_{ij} + \kappa_{ji})$$
$$+ \frac{q_{lm}\kappa_{km}}{Q}q_{ij} - \lambda Qq_{ij} + \lambda\mu q_{ij}(Q - q) \qquad (8)$$

$$\frac{\partial Q(t)}{\partial t} = -q_{ij}\kappa_{ji} - \lambda\mu Qq - \lambda Qd(1 - \mu) \qquad (9)$$

$$q = \sqrt{\sum_{ij} q_{ij}^2} \qquad (10)$$

where q_{ij} = interface tensor, κ_{ij} = velocity gradient tensor, Q = total surface area per unit volume, t = time, δ_{ij} = Kronecker delta, C_2 = constant related to the thermodynamic potential, α = interfacial tension, d, μ and λ = phenomenological parameters.

Equations (7), (8), (9) and (10) describe the evolution of the interface stress (Eq. 7), interface orientation (Eq. 8), and total surface area per unit volume (Eq. 9) during flow, giving a direct relationship between flow and morphology. λ, μ, d are three phenomenological parameters. λ is associated with how fast an interface moves when a blend is deformed, μ and d are related to the relaxation of the size and shape of the dispersed phase and range from 0 to 1, indicating the occurrence of coalescence and breakup.

In this work, the nonlinear viscoelastic behavior of PP/PS and PP/PS/SEBS blends was studied and compared to the predictions of a combination of the models of Doi and Ohta (1991), Lacroix et al. (1998) and Bousmina et al. (2001). To our knowledge this is the first time that the bulk contribution described by Lacroix et al. (1998) and the interface contribution described by Bousmina et al. (2001) have been tested at high shear rates.

The total stress tensor given by this combination of models is given by

$$\sigma_{ij} = \sigma_{ij}^{bulk} + \sigma_{ij}^{\text{interface}} - P\delta_{ij} \qquad (11)$$

where σ_{ij} = total stress tensor, σ_{ij}^{bulk} = bulk contribution tensor, $\sigma_{ij}^{\text{interface}}$ = interface contribution tensor.

Experimental

Materials and blending Commercial samples of polypropylene (PP, M_w = 350,000 g/mol with a polydispersity index PI = 4.65), polystyrene (PS, M_w = 230,000 g/mol, PI = 2.5), and Kraton G 1652 (SEBS, M_w = 72,000 g/mol, PI = 1.03), as received from suppliers, were studied. The PP/PS and PP/PS/SEBS blends were prepared using a Werner-Pfleiderer ZSK-30 twin-screw extruder, with six temperature zones, set between 190 °C and 220 °C, along the barrel. Volume fractions corresponding to 1 wt% and 10 wt% of PS were chosen to study the influence of breakup and coalescence of the dispersed phase (PS) on rheological properties. Concentrations of SEBS corresponding to 5 wt% and 10 wt% of the dispersed phase were added to the PP/PS (90/10) and PP/PS (99/01) blends, respectively. Both the PP/PS and PP/PS/SEBS blends were prepared in two steps. The compatibilizer was first mixed with the minor phase and then blended with the matrix material. In the case of the PP/PS blends the minor phase was processed twice in order to generate the same thermo-mechanical history. The homopolymers that were also tested rheologically for comparison were subjected to the same thermo-mechanical history. The nomenclature used for the blends of this work was PP/PS/SEBS (90/10/5) and PP/PS/SEBS (99/01/10).

Rheological measurements Two types of rheometer were used to study the viscoelastic behavior of the PP/PS and PP/PS/SEBS blends: a controlled strain rotational rheometer and a sliding plate rheometer. The primary objective was to determine nonlinear behavior in shear flow histories not normally used for viscoelastic characterization. For each flow history, at least three rheological measurements were performed for each material, and good reproducibility was obtained.

The first normal stress difference was determined using a controlled-strain ARES rheometer under a dry nitrogen atmosphere. A parallel-plate configuration was used with a gap of 1 mm and plate diameter of 25 mm. No correction was performed to account for shear rate non-uniformity when using parallel plate geometry. Sample discs of 25 mm diameter and 1.5 mm thickness were prepared by compression molding. For both the blends and homopolymers pellets were placed in a mold that was pressed for 25 min at a pressure of 18 MPa and a temperature of 200 °C. The time was

chosen to produce a droplet-dispersion morphology (Macaúbas and Demarquette 2001). It was verified that this procedure did not cause thermal degradation. Single-step start-up experiments were performed with all blends and homopolymers. The shear rate varied from 0.1 s^{-1} to 2 s^{-1}. For higher shear rates, sample ejection was observed. A temperature of 200 °C was used for all experiments.

Sliding plate rheometer For use in the sliding-plate rheometer, rectangular plates ($125 \times 50 \times 1$ mm) were prepared by compression molding using the same conditions as the ones used for the disc samples described above. The sliding-plate rheometer can generate large-amplitude oscillatory shear and start-up of steady shear at high rates. This rheometer can generate a broad range of shear rates (0.001 to 500 s^{-1}) at temperatures up to 300 °C. The maximum plate displacement is 100 mm, and with a plate gap of 1 mm, this implies a maximum shear strain of 100. Shear stresses up to 300 kPa are measured using a shear stress transducer (SST) (Dealy and Soong 1984; Giacomin et al. 1989). The SST senses the shear force acting on a small area in the center of the sample, thus eliminating the need to calculate the sheared area from the dimensions of the sheared sample. Also, there are no end effects. The sliding plate rheometer equipped with an SST generates homogenous shear flow in which flow instabilities are not a problem, although wall slip can occur.

Figure 1 shows the shear histories used in the sliding-plate rheometer studies. These included: single-step shear rate tests at 5 s^{-1} and 10 s^{-1} (a), as well as increasing (b), decreasing (c), reversing (d), and miscellaneous (e) sequences of shear rates. The time during which a shear rate was applied was always 10 s.

Microscopy The morphologies of unsheared and sheared samples of PP/PS and PP/PS/SEBS blends were observed using a Cambridge Stereoscan 240 scanning electron microscope (SEM). The samples were fractured in liquid nitrogen and then gold-plated using a model SCD-050 Balzers sputter coater. The size and size distribution of the dispersed phased droplets were determined by analyzing digitized photographs. The volume (R_v) and number (R_n) average radii were calculated using Eqs. (12) and (13):

$$R_v = \frac{\sum_i n_i R_i^4}{\sum_i n_i R_i^3} \tag{12}$$

$$R_n = \frac{\sum_i n_i R_i}{\sum_i n_i} \tag{13}$$

where n_i = number of droplets having the radius R_i.

No correction for the fact that the fracture surface of the droplets is not always in the middle of a droplet was performed in this work. In a previous work (Macaúbas 1999) we used Saltikov's correction (Underwood 1970). The results obtained showed that the difference between the average radius of the dispersed phase before and after correction was of less than 10% which is within experimental error.

Fig. 1a–e Shear flow histories tested using the sliding plate rheometer: **a** single step; **b** stepping up; **c** stepping down; **d** reversing; **e** multi step shear rate
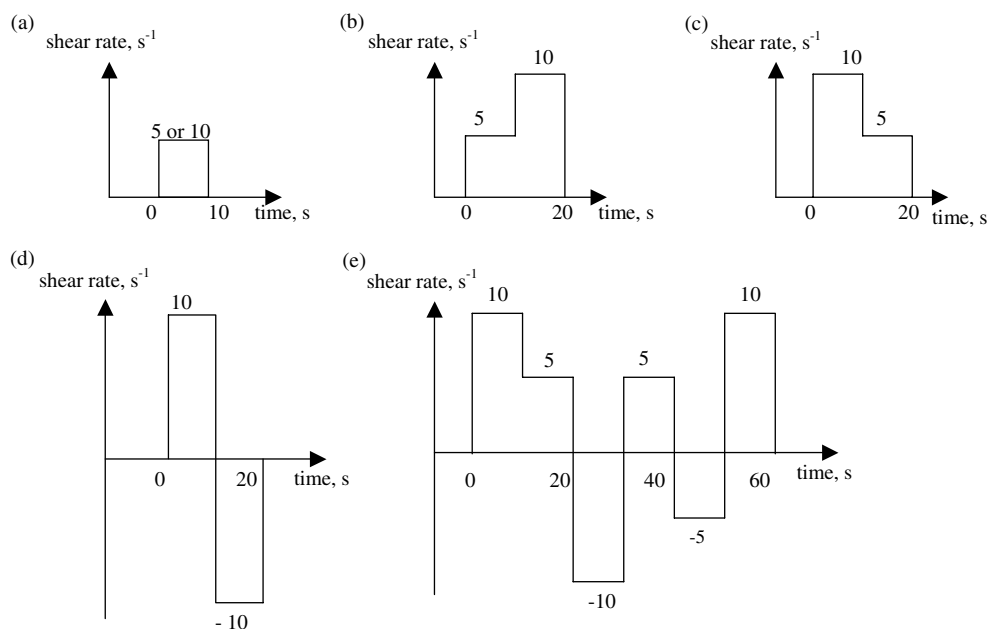
In order to remove a sheared sample from the sliding plate rheometer without damaging it, it was allowed to relax and then cooled down in situ. The temperature fell below 100 °C in less than 3 min, and the sample was pealed from the rheometer plates when its temperature was about 60 °C. The morphology quantified by Scanning Electron Microscopy (SEM) corresponded therefore to the one that is obtained after relaxation of the shape of the dispersed phase that has been sheared. No evidence of static coalescence during the three minutes lag-period was observed.

Experimental results

Morphology

Figure 2 shows a typical morphology of a blend studied in this work. A droplet-dispersion-in-a-matrix type of morphology was obtained for all the PP/PS and PP/PS/SEBS blends, and there were more small droplets than large ones. Neither the type of morphology nor the shape of the droplet size distribution was changed significantly after applying the shear flow histories tested in this work.

Table 1 quantifies the evolution of morphology according to the shear flow history in the sliding plate
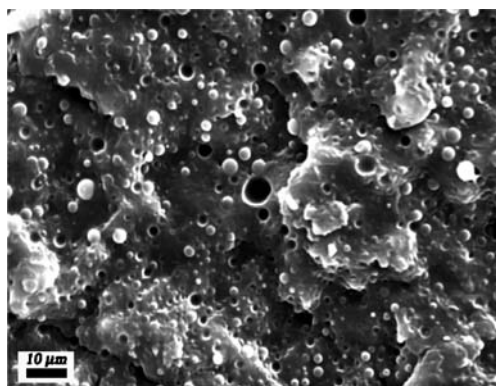
rheometer (SPR) based on the volume averaged radius and polydispersity (R_v/R_n).

Single-step shear rate tests

Figures 3 and 4 show the behavior of the shear stress and first normal shear stress difference, respectively, for blends PP/PS (90/10) and PP/PS/SEBS (90/10/5) when subjected to single-step shear rate deformations. Similar results were obtained for the other blends and single-phase systems.

It can be seen that a stress overshoot typical of nonlinear viscoelastic behavior was observed at short times, followed by a steady state region for shear rates higher than 0.1 s^{-1}. At a shear rate of 0.1 s^{-1} no stress overshoot was observed. The first normal stress difference increased with time and then leveled off. In the case of the sliding plate rheometer, plate displacement was the factor limiting the duration of an experiment. In the case of the ARES rheometer, data were recorded until the shear stress reached a steady state. In Fig. 4, first normal stress difference data are shown only for shear rates from 0.1 to 2 s^{-1}, corresponding to the useful range of the ARES rheometer. The sliding-plate rheometer

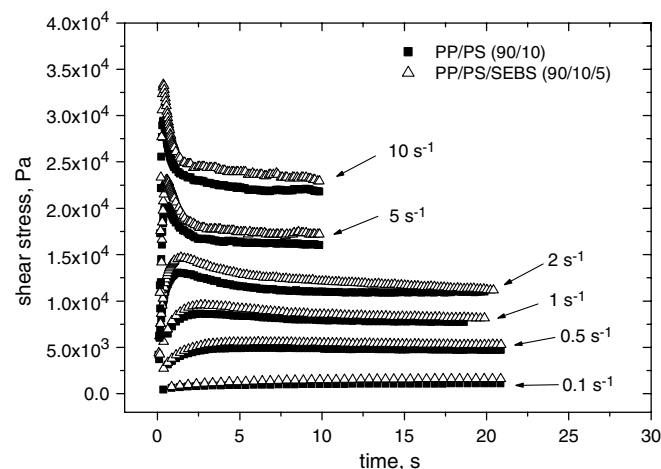Fig. 2 Typical morphology of blend studied in this work

Fig. 3 Shear stress behavior for single step shear rate tests

Table 1 Morphology evolution for the various shear histories in the SPR

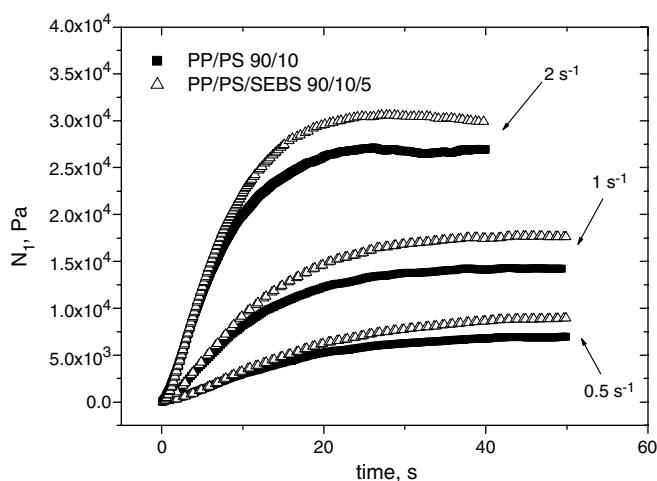| Flow Blends	Before		5 s^{-1}		10 s^{-1}		5 and 10 s^{-1}		10 and 5 s^{-1}		10 and −10 s^{-1}		Multi step	
	R_v (μm)	R_v/R_n	R_v (μm)	R_v/R_n	R_v (μm)	R_v/R_n	R_v (μm)	R_v/R_n	R_v (μm)	R_v/R_n	R_v (μm)	R_v/R_n	R_v (μm)	R_v/R_n
90/10	1.41	1.40	1.31	1.17	1.24	1.69	0.91	1.43	1.14	1.60	1.21	1.58	1.28	1.65
90/10/5	0.69	1.53	0.68	1.51	0.68	1.38	0.59	1.58	0.62	1.31	0.60	1.63	0.84	1.63
99/01	0.37	1.23	0.34	1.32	0.34	1.35	0.36	1.16	0.34	1.22	0.42	1.27	0.37	1.20
99/01/10	0.26	1.20	0.22	1.09	0.22	1.15	0.27	1.12	0.25	1.12	0.24	1.20	0.31	1.19

Fig. 4 First normal stress difference for single step shear rate tests

was equipped with a transducer that permitted only shear stress measurements.

Double and multi-step shear rate

Double-step shear rate tests with the shear rate increasing from 5 s^{-1} to 10 s^{-1}, decreasing from 10 s^{-1} to 5 s^{-1}, and reversing from 10 s^{-1} to −10 s^{-1}, were performed for all blends and pure components. Figures 5 and 6 show the shear stress for PP/PS (90/10) and PP/PS/SEBS (90/10/5) when subjected to double step shear rate with the shear rate decreased from 10 to 5 s^{-1}, and to multi-step shear rate tests as representative examples of the behavior observed. Similar results were obtained for the other blends and single phase systems.
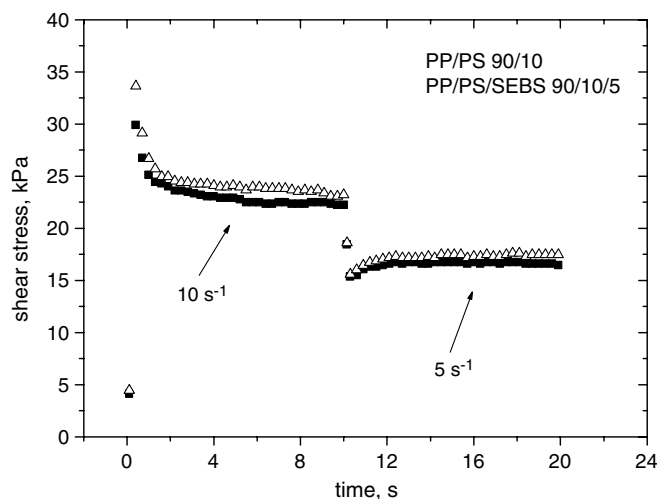

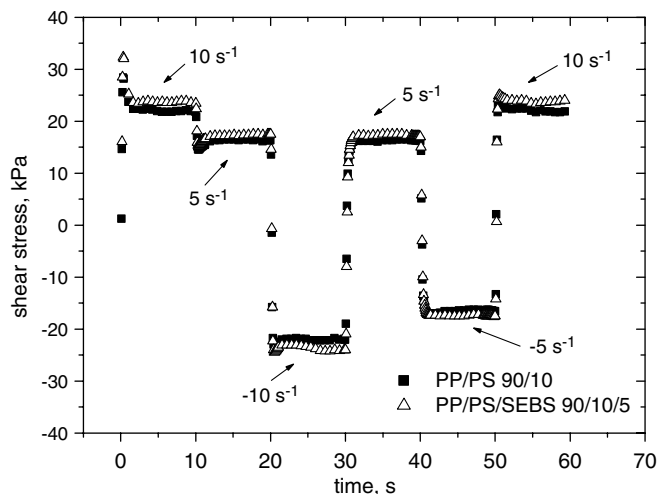**Fig. 5** Shear stress behavior when decreasing the shear rate

Fig. 6 Shear stress behavior when varying the shear rate

When the shear rate increases from 5 s^{-1} to 10 s^{-1}, a second stress overshoot appeared after the shear rate change, followed by a new steady-state. And when the shear rate decreases from 10 s^{-1} to 5 s^{-1}, after the change of shear rate there was a stress undershoot, followed by a new steady-state. Finally, when the shear rate was reversed from 10 s^{-1} to −10 s^{-1}, after the change of shear rate there was a stress undershoot, followed by a steady stress whose magnitude is equal to that after the first step. When a more complex shear history was applied to the PP/PS and PP/PS/SEBS blends and their pure components, stress overshoots and undershoots were observed, according to the shear rate transitions. For the materials studied in this work, no overshoot or undershoot was observed from the third to fourth and fourth to fifth shear rate steps. As in the double-step shear rate tests, the steady state stress for subsequent steps were quite close to the ones for the first step at 5 or 10 s^{-1}, for a given final shear rate.

Discussion

Morphology

Table 1 shows the variation of volume average (R_v) and polydispersity (R_v/R_n) for all blends submitted to the different flow histories studied in this work. The results indicate that for every shear flow history, there is a slight decrease of the volume average radius (R_v) for the PP/PS (90/10) blend which is expected as for shear rates of 5 s^{-1} and 10 s^{-1} the capillary number ($Ca = \frac{\eta_m R \dot{\gamma}}{\alpha}$ where Ca = capillary number, η_m = matrix viscosity, R = droplet radius, $\dot{\gamma}$ = shear rate, α = interfacial tension) is higher (3.21 at 5 s^{-1} and 4.83 at 10 s^{-1}) than the critical capillary number for breakup (which is of the order of 0.5 for

both shear rates) that can be calculated using the expression derived by de Bruijin (1989) and given by

$$\log(Ca_{cri}) = -0.506 - 0.0994 \log(K) + 0.124 \log^2(K) - \frac{0.115}{\log(K) - \log(4.08)}$$

$$(14)$$

where Ca_{cri} = critical capillary number, K = viscosity ratio.

In the case of the PP/PS/SEBS (90/10/5) blend no significant variation of the volume-averaged radius (R_v) in the single step shear rate tests of 5 s^{-1} and 10 s^{-1} was observed. The fact that the morphology is unchanged is probably due to a steric effect of SEBS, which prevents the coalescence of PS droplets. For compatibilized blends the steady shear capillary number is expected to be larger than the Ca_{cri} for uncompatibilized ones, i.e. the hydrodynamic stress needed for droplet break-up is higher than the one coming from the action of interfacial tension (Velankar et al. 2001, 2004), thus PS droplets encapsulated by SEBS are expected to be more resistant to the shear deformation. Also, the shear rates may not be high enough to break up the higher viscosity dispersed phase droplets (the viscosity of PS + SEBS is higher than that of PS).

When the shear rate was increased, decreased or reverted, there was a decrease of the volume-averaged radius (R_v), probably due to the more severe shear deformation promoted. In the multi-step shear rate tests there was an increase in the volume-averaged radius (R_v). It is possible that for a more complex shear flow history, in which both the magnitude and the sign of the shear rate change, the SEBS may lose its efficiency by its partial removal from the interface between the droplets and matrix, which in turns allows coalescence among PS

droplets. Jeon and Macosko (2003) studied the effect of shear deformation on a fluorescent-labeled poly(styrene-*b*-methylmethacrylate) (NBD-PS-*b*-PMMA) block copolymer on the surface of a polymethylmethacrylate (PMMA) drop in a polystyrene (PS) matrix and observed a non-uniform copolymer distribution around the deformed droplet after deformation. The non-uniform distribution was characterized by higher concentrations of block copolymer in regions of high curvature (edges and tips). In a similar fashion, the high shear generated during the multiple step shear rate tests may have caused a redistribution of SEBS around the dispersed phase and even a partial removal from the interface, leading to coalescence, once the total strain caused by the shearing ($\gamma = 450$) is much greater than those applied (lower than $\gamma = 20$) by Jeon and Macosko (2003).

In the case of blends PP/PS (99/01) and PP/PS/SEBS (99/01/10) no significant variation of the volume averaged (R_v) radius was observed for any shear history. In this case, the capillary numbers were hardly larger than the Ca_{cri} (0.84 at 5 s^{-1} and 1.2 at 10 s^{-1}). Also, the small volume fraction of the dispersed phase probably does not favor coalescence due to the small probability of two droplets interacting. Also, very small droplets when deformed have the ability to relax very fast, recovering their initial shape without breaking up. Table 1 also shows that for all blends and shear histories, the polydispersity was not significantly altered by the shear.

Single shear rate step

Figure 7 shows a possible morphology evolution during the application of a single-step shear rate to PP/PS and PP/PS/SEBS blends. The total dispersed phase is assumed to be a single drop that suffers deformation.

Fig. 7 Sketch of possible morphology evolution during single step shear rate
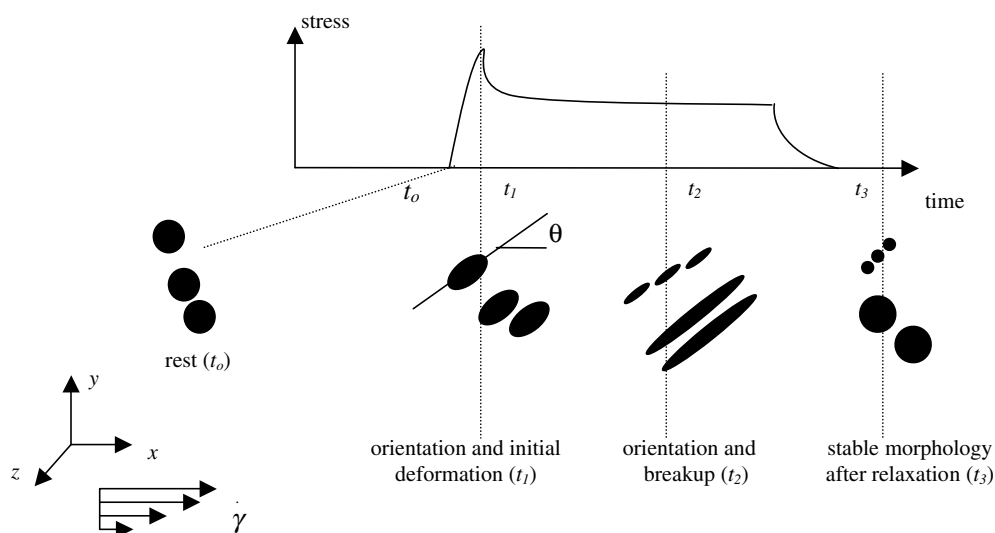
Such an assumption has already been made by Bousmina et al. (2001) to represent qualitatively the evolution of blend morphology under shear. The drawings are purely qualitative. The geometrical features of the ellipses weren't measured nor theoretically predicted.

The dispersed-phase drop is initially spherical, but as shearing begins it slightly deforms into an ellipsoid having a principal axis at an orientation angle θ with respect to the direction of shear, at the time of stress overshoot (t_1). After the stress overshoot time (t_1) the deformed droplet reaches its maximum orientation and then continues to stretch. For small deformation, this maximum orientation is 45° and can be higher for larger deformations. For times greater than (t_1), the shear stress decreases and levels off. During this time the droplet continues deforming and may break up or coalesce with other droplets. As soon as the deformation stops, the deformed droplet relaxes until it reaches a new state of equilibrium (t_2). In the case of the experiments presented here (for the uncompatibilized blends) the average size of the dispersed phase after shear is smaller

than the one at (t_o), indicating that droplet breakup has occurred.

Table 2 shows the times of overshoot and overshoot and the steady state shear stresses and first normal stress differences for all the materials subjected to single-step shear rate tests.

Good reproducibility of viscoelastic properties was obtained for all the systems studied. For the times at which the overshoot occurred, the standard deviation divided by the mean ranged from 1.4% to 7.1%. The same ratio was found to range from 1.3% to 8.3% for the stress overshoot, from 1.1% to 5.5% for the steady-state shear stress, and from 0.56% to 2.1% for the first normal stress difference.

Table 2 shows that the time at which stress overshoot occurs for PP is higher than that for PS at all shear rates. At 0.5 s^{-1}, the stress overshoot time of the blend is higher than that of either pure component, showing that the overshoot is a result of the two-phase character of the blend. As the shear rate increases, the time at which overshoot occurs decreases and approaches that of PP,

Table 2 Summary of results for single-step shear rate tests

Rate (s^{-1})	Material	Overshoot time (s)	Overshoot stress (kPa)	Steady state stress (kPa)	N_1 steady state (kPa)
0.1	90/10	-	-	1.10	No steady state
	90/10/5	-	-	1.68	1.40
	99/01	-	-	1.09	No steady state
	99/01/10	-	-	1.22	0.95
	PP	-	-	1.07	0.48
	PS	-	-	0.88	0.56
0.5	90/10	6.63	4.95	4.70	7.18
	90/10/5	6.13	5.90	5.09	9.24
	99/01	7.07	4.61	4.43	4.95
	99/01/10	8.13	4.70	4.49	5.40
	PP	5.77	4.51	4.34	4.06
	PS	4.06	3.73	3.27	4.03
1	90/10	2.63	8.62	7.62	14.0
	90/10/5	2.63	9.78	7.76	17.6
	99/01	3.38	8.16	7.25	11.1
	99/01/10	3.38	8.44	7.86	12.3
	PP	3.17	7.55	7.24	6.67
	PS	2.16	6.40	5.42	9.79
2	90/10	1.33	13.1	11.2	26.6
	90/10/5	1.53	14.7	12.2	30.3
	99/01	1.68	12.4	10.9	23.0
	99/01/10	1.38	13.1	12.0	22.8
	PP	1.95	11.6	10.7	16.6
	PS	1.21	11.7	9.71	18.0
5	90/10	0.56	21.36	16.61	x
	90/10/5	0.54	23.76	17.37	x
	99/01	0.59	18.79	16.86	x
	99/01/10	0.60	20.81	17.64	x
	PP	0.60	18.22	16.10	x
	PS	0.46	22.06	16.12	x
10	90/10	0.35	29.81	22.03	x
	90/10/5	0.35	33.05	23.68	x
	99/01	0.36	27.08	23.76	x
	99/01/10	0.37	30.00	25.33	x
	PP	0.36	26.13	21.72	x
	PS	0.22	30.62	20.27	x

-: no overshoot time and stress observed
x: not available in the sliding plate rheometer

which implies that the matrix phase dominates the rheological behavior of the blend.

Figure 8 shows the time of overshoot as function of the reciprocal of the shear rate. We see that the time of overshoot scales linearly with the reciprocal of the shear rate, indicating that the stress overshoot occurs at constant strain. Osaki et al. (1976) and Demarquette and Dealy (1992) observed similar behavior for concentrated solutions of polystyrene. The results reported here indicate that the maximum orientation of the dispersed phase with respect to the direction of shear occurs at a fixed value of strain.

Table 2 shows that the overshoot time is not affected by the presence of SEBS, indicating that the addition of SEBS does not change the orientation angle and initial deformation mechanism of the dispersed phase. Similar results were reported by Iza et al. (2001). Also, the overshoot and steady-state stresses for the compatibilized blends are larger than the ones for the uncompatibilized blends. This is probably related to the compatibilizing efficiency of SEBS. Macaúbas and Demarquette (2001) observed by use of transmission electron microscopy and an SEBS staining technique that the PS droplets are encapsulated by SEBS, forming a core-shell structure that promotes strong adhesion between the dispersed phase and the matrix. A direct consequence of this morphology is the viscosity increase of the compatibilized blend, compared to that of the uncompatibilized blend, even though low concentrations of compatibilizer were used (5 wt% and 10 wt% with respect to the minor phase PS).

The theory developed by Doi and Ohta (1991) predicts that in steady shear both the shear stress and first normal stress difference follow the scaling relationship given by Eq. (4) and consequently are proportional to the shear rate, i.e.

$$\sigma \propto \dot{\gamma} \tag{15}$$

$$N_1 \propto |\dot{\gamma}| \tag{16}$$

Figure 9 shows the steady-state shear stress as a function of shear rate for a PP/PS (90/10) blend. It can be clearly seen from Fig. 9, that the shear stress is not proportional to the shear rate for the range of shear rates studied in this work. Similar results were observed for the other PP/PS, PP/PS/SEBS blends, as well as for the pure PP and PS. The curve profile of steady-state shear stress observed in Fig. 9 is similar to the one predicted by Yu et al. (2002) for the interface contribution. These authors predicted that the interface contribution is proportional to the shear stress only at low shear rates.

Figure 10 shows the first normal stress difference for the PP/PS and PP/PS/SEBS blends and pure components as functions of shear rate. The steady-state value of the first normal stress difference follows fairly closely the prediction of the Doi-Ohta theory. The same behavior was observed for all the materials studied.

Figure 11 shows the contribution of the interface to the steady-state shear stress as a function of shear rate for PP/PS and PP/PS/SEBS blends. The interface contribution to the stress was determined by subtracting the bulk contribution, calculated using Eqs. (5) and (6), from the measured total shear stress.

One must be careful in selecting a mixing rule to calculate the contribution of the interface. Since the bulk normally accounts for most of the total stress, the use of an inaccurate mixing rule can lead to a large error in the interface contribution. The mixing rule of Lacroix et al. (1998) is an improvement on that of Lee and Park (1994), who used the mismatch of viscosities to predict the rheological behavior of blends undergoing
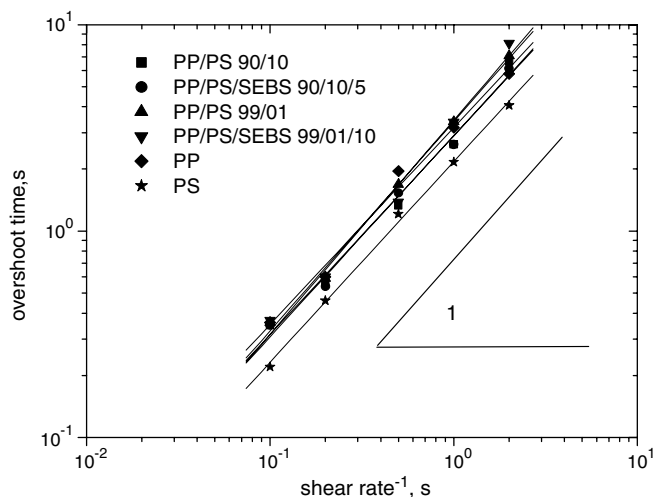

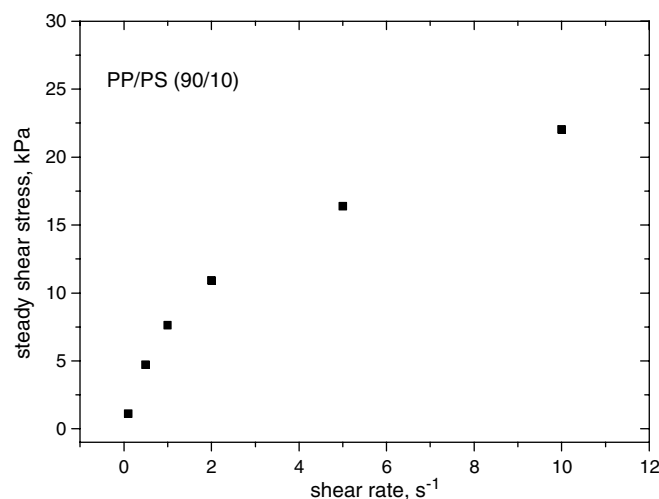Fig. 8 Overshoot time as function of the reciprocal shear rate

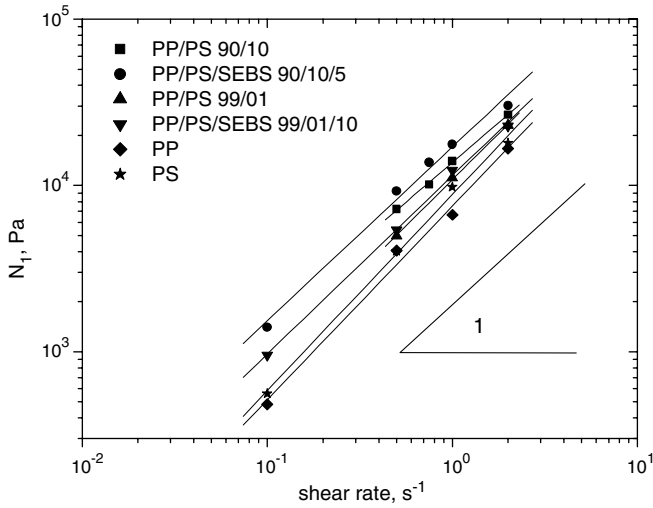Fig. 9 Steady-state shear stress as a function of shear rate

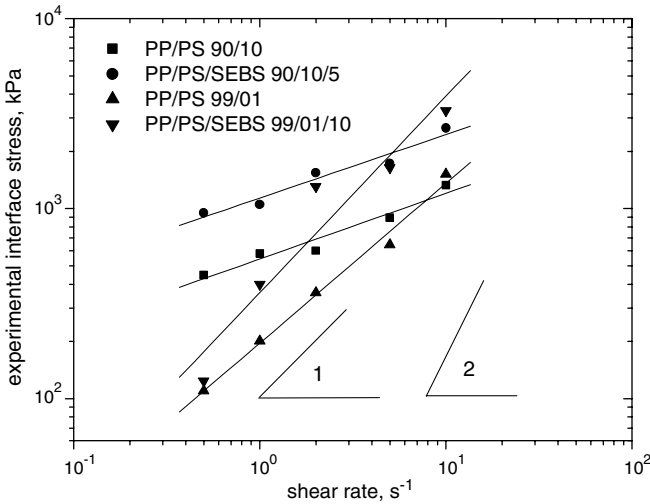**Fig. 10** First normal stress difference as function of the shear rate

Fig. 11 Contribution of interface to the steady stress shear stress

deformation. The mixing rule of Lacroix et al. (1998) has the advantage that is does not rely on empirical relationships such as the Cox-Merz rule. However, the results indicate that for large shear rates (5 and 10 s^{-1}) the interface contribution to the total stress for a 1% disperse phase is comparable in magnitude to the one for a 10% disperse phase. Mathematically this can be explained as follows: a) for these shear rates values (5 and 10 s^{-1}) the viscosity ratio η_d/η_m (where η_d is the viscosity of the dispersed phase and η_m is the viscosity of the matrix phase) is almost equal to one, resulting in a bulk composition to the total stress that is comparable in magnitude to $\eta_m\dot{\gamma}_{ij}$ (where η_m is the viscosity of the matrix phase, and $\dot{\gamma}_{ij}$ is the shear rate); b) experimentally the total stress for both blends (90/10 and 99/01) at 5

and 10 s^{-1} are comparable in magnitude. Since the interface contribution to the total stress is obtained by subtracting the bulk stress from the total stress, the interface contributions for both blends are of the same order of magnitude. However, no physical explanation could be found for this behavior suggesting that the equation used for calculating the bulk contribution should take other parameter into consideration.

Figure 11 shows that only in the case of blend PP/PS (99/01) was a linear scaling law valid. This result differs from the experimental results of Takahashi et al. (1994a, 1994b) and the theoretical predictions of Bousmina et al. (2001). Takahashi et al. (1994a, 1994b) reported that the contribution of the interface to the total steady shear stress scales linearly with shear rate. Bousmina et al. (2001) predicted that this same scaling law is valid only after a critical shear rate.

Double and multi-step shear rates

The stress overshoots and undershoots and times at which they occur for the second (in the case of double-step shear rate) and subsequent (in the case of multi-step shear rates) were compared to those obtained in single step shear rate tests. It was observed that for all the double-step shear histories (increasing, decreasing and reversing shear rates) the stress overshoot or undershoot corresponding to the second shear rate were lower than the value for a single-step shear rate. For example, when the shear rate increased from 5 to 10 s^{-1} the second stress overshoot showed a variation of −19% for the PP/PS (90/10) blend, −20% for the PP/PS/SEBS (90/10/5), −12% for the PP/PS (99/01) blend, and −10% for the PP/PS/SEBS (99/01/10) blend, whereas for the pure phases it was −4.4% for PP and −34% for PS. When the shear rate was decreased from 10 to 5 s^{-1} the variation of stress undershoot was −28%, −34%, −7.3%, −20%, −18% and −52% for the same materials sequence. It was also observed that: a) the time at which the stress over-shoot/undershoot occurs decreased both when the shear rate increased and decreased, if the direction of shear is not changed, for example when the shear rate increased from 5 to 10 s^{-1} there was a variation of −8% in this time for the PP/PS (90/10) blend, −14% for the PP/PS/SEBS (90/10/5) blend, −17% for the PP/PS (99/01), −19% for the PP/PS/SEBS (99/01/10) blend, −11% for PP and −9.1% for PS, when the shear rate was decreased from 10 to 5 s^{-1} the variation and of undershoot time was −30%, −34%, −34%, −33%, −40% and −28% for the same materials sequence; b) the time at which stress under-shoot occurs increased when the direction of flow was reversed, there was an increase of 160% for the PP/PS (90/10) blend, 114% for the PP/PS/SEBS (90/10/5), 56% for the PP/PS (99/01) blend, 62% for the PP/PS/SEBS (99/01/10) blend, 77% for PP and 186% for PS.

The variations in the overshoot and undershoot times and stresses for the subsequent shear rate steps of double and multi-step shear rate tests cannot be attributed solely to the rheological behavior of the individual phases, as the variation of stress overshoot and time of overshoot for the blends are quite different from those of the pure phases. Such variations can provide a qualitative insight regarding the mechanism of initial deformation and orientation of the dispersed phase of PP/PS and PP/PS/SEBS with respect to the direction of shear.

Figure 12 is a sketch of a possible morphology evolution for a reduction in shear rate. During the first shear rate (10 s^{-1}), the morphology evolves according to the description of Fig. 5. At the change of shear rate (t_1), the already deformed and oriented (θ_1) dispersed phase is subjected to the new shear rate (5 s^{-1}) and is reoriented to a new angle (θ_2) with the direction of shear. The lower values of stress undershoot and the time at which it occurs after time t_1 when compared with the corresponding values in single-step shear at a rate at 5 s^{-1} could be a result of the orientation and deformation state of the dispersed phase resulting from the first shear rate (10 s^{-1}), which would cause faster orientation at a lower level of stress undershoot.

Figure 13 shows a possible morphology evolution for the case of reversing shear direction. At the change of shear rate (t_1) the dispersed phase may undergo a change in shape, with posterior reorientation at time t_2 similar to that described by Hayashi et al. (2001). Using a visualization technique, Hayashi et al. (2001) studied the recovery process of a single droplet of poly(isobutylene) (PIB) immersed in a matrix of poly(dimethylsiloxane) (PDMS) during the application of large double-step shear strain in opposite directions. Hayashi et al. (2001) found that when the second step shear strain was applied, a droplet already deformed into a rod-like shape assumed a complex variety of shapes until finally taking on a shape that they called a "hamburger-like" droplet, which had more than one orientation angle. Similarly, in the present study, when the shear rate is reversed from 10 s^{-1} to -10 s^{-1}, the dispersed phase particles in PP/PS and PP/PS/SEBS blends can assume complex shapes that require additional time to reach an equilibrium orientation angle, thus resulting in an increase in the undershoot time. Comparing the response of the blends in various shear histories for the same total strain, such as increasing the shear rate from 5 to 10 s^{-1} and decreasing the shear rate from 10 to 5 s^{-1}, quite different overshoot characteristics were observed. For all PP/PS and PP/PS/SEBS blends, as well as for pure PP and PS, there was a larger effect on the overshoot characteristics when decreasing the shear rate than when increasing it.

The tendency to increase the overshoot/undershoot times when the shear rate is reversed is maintained for the miscellaneous of shear rates. However, the magnitude of this increase is lower than the one found for the reverse double step shear rate test for all materials studied. Also, there was a sequential decrease of the stress overshoot as long as the step shear rates were applied to the samples. Moreover, during the transition from the fourth (5 s^{-1}) to the fifth (-5 s^{-1}) shear rate it was not possible to identify a stress overshoot or undershoot. Even at a qualitative level, we cannot state that the mechanism of deformation for the multi-step

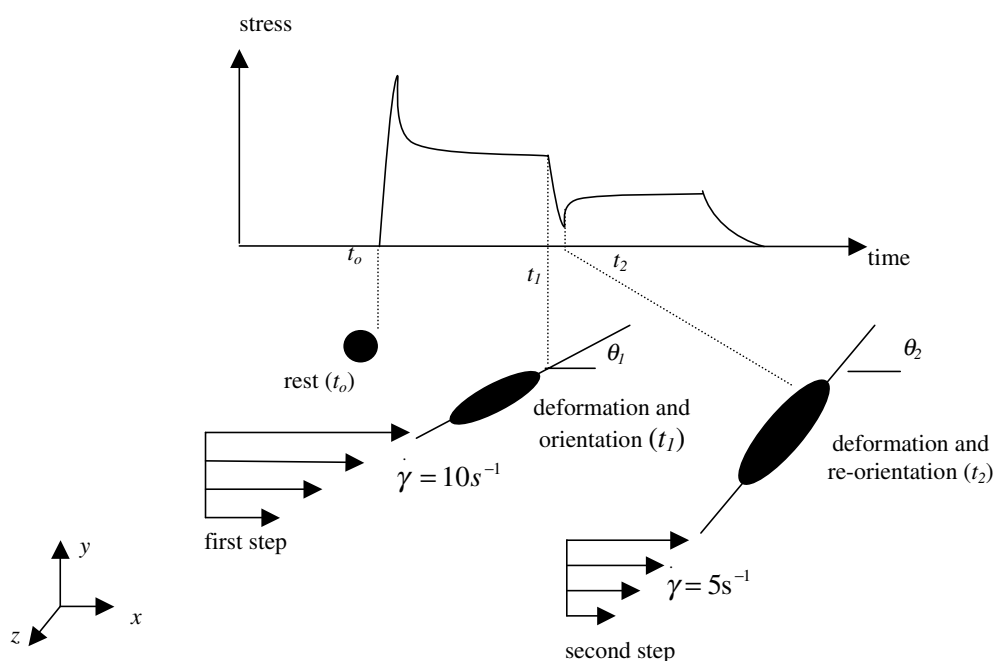Fig. 12 Sketch of possible morphology evolution when stepping down the shear rate
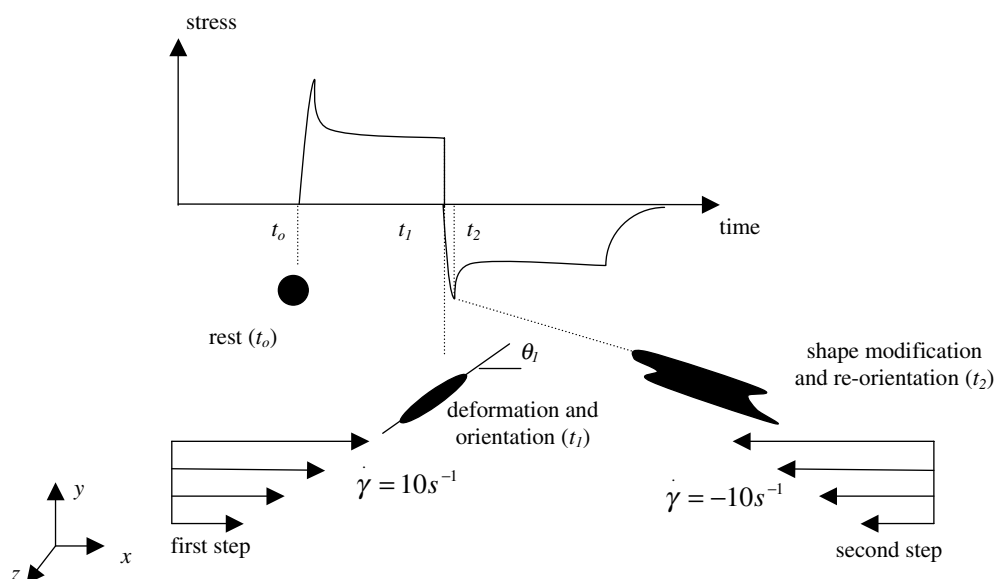
Fig. 13 Sketch of possible morphology evolution when reversing the shear rate

shear rate tests follow necessarily the mechanism depicted in Figs. 7, 12 and 13, once they do not take into account the absence of some undershoots and overshoots in Fig. 6.

Table 3 compares values of the steady-state stress after the second step shear rate with the corresponding steady-state stress in a single step shear rate test, which are indicated in bold type.

The steady-state stresses for the second step are statistically equal to those occurring in the single shear rate tests. This result was obtained for all the materials subjected to double- and multi-step shear rate tests. Although the morphology of the blends changed during the flow, the variation observed was probably too small to affect the values of shear stresses. In addition, the double and multi-step shear rate and tests showed that the scaling law between the shear stress and shear rate predicted by Doi and Ohta (1991) is not obeyed, i.e. when doubling the shear rate the shear stress is not doubled.

Modeling

Single-step shear rate

The shear stress data were compared with the prediction of the model formulated by combining concepts in the Doi and Ohta (1991), Lacroix et al. (1998) and Bousmina et al. (2001) theories. The general expression of Doi and Ohta was used for the total stress, the bulk contribution was calculated according to Lacroix et al. (1998) (Eqs. 5 and 6), and the interface contribution was that proposed by Bousmina et al. (2001) (Eqs. 7, 8, 9 and

Table 3 Steady-state shear stresses

Rates (s^{-1})	Material	Second steady state (kPa)
5 and 10	90/10	22.63 ± 1.69
		(22.03 ± 0.59)
	90/10/5	23.81 ± 0.6
		(23.68 ± 0.42)
	99/01	23.47 ± 0.24
		(23.76 ± 0.32)
	99/01/10	24.95 ± 0.39
		(25.33 ± 0.76)
	PP	22.47 ± 1.15
		(21.72 ± 0.96)
	PS	20.64 ± 0.17
		(20.27 ± 0.45)
10 and −10	90/10	-22.63 ± 1.69
		(22.03 ± 0.59)
	90/10/5	-23.81 ± 0.46)
		(23.68 ± 0.42
	99/01	-23.55 ± 1.22
		(23.76 ± 0.32)
	99/01/10	-24.95 ± 0.39
		(25.33 ± 0.76)
	PP	-22.47 ± 1.15
		(21.72 ± 0.96)
	PS	-20.64 ± 0.17
		(20.27 ± 0.45)
10 and 5	90/10	16.52 ± 0.82
		(16.61 ± 0.68)
	90/10/5	17.40 ± 0.45
		(17.37 ± 0.95)
	99/01	16.88 ± 0.23
		(16.86 ± 0.93)
	99/01/10	17.47 ± 0.06
		(17.64 ± 0.20)
	PP	15.88 ± 0.60
		(16.10 ± 0.70)
	PS	9.23 ± 0.93
		(16.12 ± 0.46)

Bold face numbers are from single-step tests

10). For the calculation of the bulk contribution to the PP/PS blends, the shear rate dependent viscosities of PP and PS single phases were taken into account, and in the case of the PP/PS/SEBS blends, mixtures of PS/zSEBS (5 wt% and 10 wt% with respect to PS wt% phase) were taken to be the dispersed phases. For the quantification of the interface contribution, two assumptions were made: C_2 was set equal to zero, and values of λ, μ, d were determined by fitting the experimental total stress data to Eq. (11). It has been reported in the literature that the use of C_2 is of the order of 10^{-12} to 10^{-8} N (Lacroix et al. 1998, 1999; Bousmina et al. 2001).

When the second term on the right hand side of Eq. (7), $\left[2C_2\left(\frac{2}{3}Q + 2q_{kj} - \frac{q_{ml}^2}{Q}\right)q_{ji}\right]$, was evaluated it was found to be several orders of magnitude smaller than the first term of the right hand side, αq_{ij}. Therefore, the second term on the right hand side of Eq. (7) was neglected in the calculation of the interface contribution.

Therefore, in order to evaluate the contribution of the interface, the following system of equations was solved:

$$\frac{\partial q_{11}(t)}{\partial t} = \frac{2}{3}q_{12} + \frac{q_{12}q_{11}}{Q} - \frac{\lambda(1-\mu)Qq_{11}}{\dot{\gamma}}$$
$$- \frac{\lambda\mu(\sqrt{q_{11}^2 + 2q_{12}^2 + q_{22}^2 + q_{33}^2})q_{11}}{\dot{\gamma}} \quad (17)$$

$$\frac{\partial q_{12}(t)}{\partial t} = -q_{11} - \frac{1}{3}Q + \frac{q_{12}^2}{Q} - \frac{\lambda(1-\mu)Qq_{12}}{\dot{\gamma}}$$
$$- \frac{\lambda\mu(\sqrt{q_{11}^2 + 2q_{12}^2 + q_{22}^2 + q_{33}^2})q_{12}}{\dot{\gamma}} \quad (18)$$

$$\frac{\partial q_{22}(t)}{\partial t} = -\frac{4}{3}q_{12} + \frac{q_{12}q_{22}}{Q} - \frac{\lambda(1-\mu)Qq_{22}}{\dot{\gamma}}$$
$$- \frac{\lambda\mu(\sqrt{q_{11}^2 + 2q_{12}^2 + q_{22}^2 + q_{33}^2})q_{22}}{\dot{\gamma}} \quad (19)$$

$$\frac{\partial q_{33}(t)}{\partial t} = \frac{2}{3}q_{12} + \frac{q_{12}q_{33}}{Q} - \frac{\lambda(1-\mu)Qq_{33}}{\dot{\gamma}}$$
$$- \frac{\lambda\mu(\sqrt{q_{11}^2 + 2q_{12}^2 + q_{22}^2 + q_{33}^2})q_{33}}{\dot{\gamma}} \quad (20)$$

$$\frac{\partial Q(t)}{\partial t} = -q_{12}$$
$$- \lambda Q\left(\frac{d(1-\mu) + \mu}{\dot{\gamma}}\right)\sqrt{q_{11}^2 + 2q_{12}^2 + q_{22}^2 + q_{33}^2} \quad (21)$$

with initial conditions $q_{ij}(0) = 0$ and $Q(0) = \frac{3\phi}{R_v}$ where q_{ij} = interface tensor, Q = total surface area per unit of volume, t = time, d, μ, λ = phenomenological parameters,

φ = volume fraction of the dispersed phase, R_v = volume average radius.

The initial values of the phenomenological parameters were set so that the profile of the interface contribution $q_{12}(t)$ was given by an overshoot followed by a steady state, as would be expected for the rheological behavior of the experimental total stress and the bulk contribution. Then the values of the phenomenological parameters were refined by minimization of the standard deviation between the steady-state values of the experimental and predicted shear stress. It was not possible to obtain a good fit between experimental and predicted shear stress by the optimization of the stress overshoot. Table 4 shows the fitted values of the phenomenological parameters for the PP/PS and PP/PS/SEBS blends subjected to single-step shear rate tests.

Figure 14 shows the total shear stress together with the bulk and experimental interface contributions for a PP/PS (90/10) blend at 10 s^{-1}. The latter contribution was calculated by subtracting the bulk contribution given by Lacroix et al. (1998) from the total shear stress. Similar results were observed for the other blends.

We see that the bulk contribution plays a major role in the rheological behavior, mainly as a result of the volume fractions of 1% and 10% used in this work. A reliable mixing rule is thus an essential element of a successful model. In addition, during modeling it was found that the predicted interface contribution always underestimated the experimental one. Also, there was a significant difference between the experimental

Table 4 Values of phenomenological parameters fitted to data

| Rate (s^{-1})	Blend	$\lambda(10^{-7}$m/s)	μ	d
0.1	90/10	0.92	0.87	0.72
	90/10/5	0.79	0.12	0.73
	99/01	0.83	0.90	0.97
	99/01/10	0.57	0.77	0.62
0.5	90/10	1.10	0.55	0.93
	90/10/5	1.01	0.57	0.77
	99/01	0.90	0.89	0.97
	99/01/10	0.90	0.96	0.98
1	90/10	1.50	0.67	0.95
	90/10/5	1.38	0.66	0.79
	99/01	1.05	0.89	0.98
	99/01/10	1.15	0.88	0.90
2	90/10	2.20	0.75	0.96
	90/10/5	1.90	0.74	0.81
	99/01	2.10	0.90	0.97
	99/01/10	1.65	0.91	0.91
5	90/10	3.78	0.82	0.95
	90/10/5	3.30	0.80	0.83
	99/01	3.10	0.94	0.98
	99/01/10	2.51	0.94	0.93
10	90/10	4.83	0.88	0.96
	90/10/5	4.62	0.85	0.84
	99/01	3.85	0.96	0.98
	99/01/10	2.99	0.97	0.96
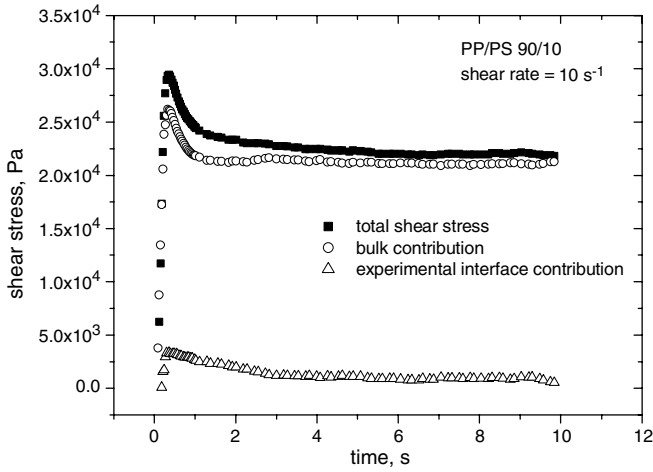
Fig. 14 Comparison between total shear stress, and contributions of bulk and interface for a PP/PS 90/10 blend submitted to a shear rate of 10 s^{-1}

overshoot time and the overshoot time of the predicted interface contribution, which could be related to a deficiency in the description of overshoot features. For example, at 10 s^{-1} the time at which overshoot was observed for the PP/PS (99/01) blend was 0.36 s (Table 2), and its interface contribution reached its overshoot at 6.7 s. Table 5 shows the ratios between predicted and experimental interface contributions.

It can be seen that the higher the shear rate the poorer the ability of the model to describe the interface contribution. And the situation is worse for the compatibilized blends.

Figure 15a,b shows comparisons between the experimental and predicted shear stresses for the PP/PS (90/10) and PP/PS/SEBS (90/10/5) blends, respectively. Similar results were obtained for the PP/PS (99/01) and PP/PS/SEBS (99//01/10) blends.

Figure 15a shows that the shear stress behavior of PP/PS blends was reasonably well described by the combination of nonlinear models for shear rates

between 0.1 s^{-1} and 1 s^{-1}. For higher shear rates the models underestimated the stress overshoot. At a shear rate of 0.1 s^{-1} there was a prediction of an overshoot coming from the interface contribution, which was not found experimentally.

Figure 15b reveals that the agreement is not good for the compatibilized blends. This is probably because the combination of nonlinear models employed does not take into account the presence of a compatibilizer. Additional stresses would be expected to arise from the modification of interface by a compatibilizer, and an accurate prediction would require a complex boundary condition that is not included in the emulsion models used here.

Figures 16 and 17 show the long-term (beyond the experimental time range) prediction of the normalized total surface area per unit volume ($Q(t)/Q(0)$) for the
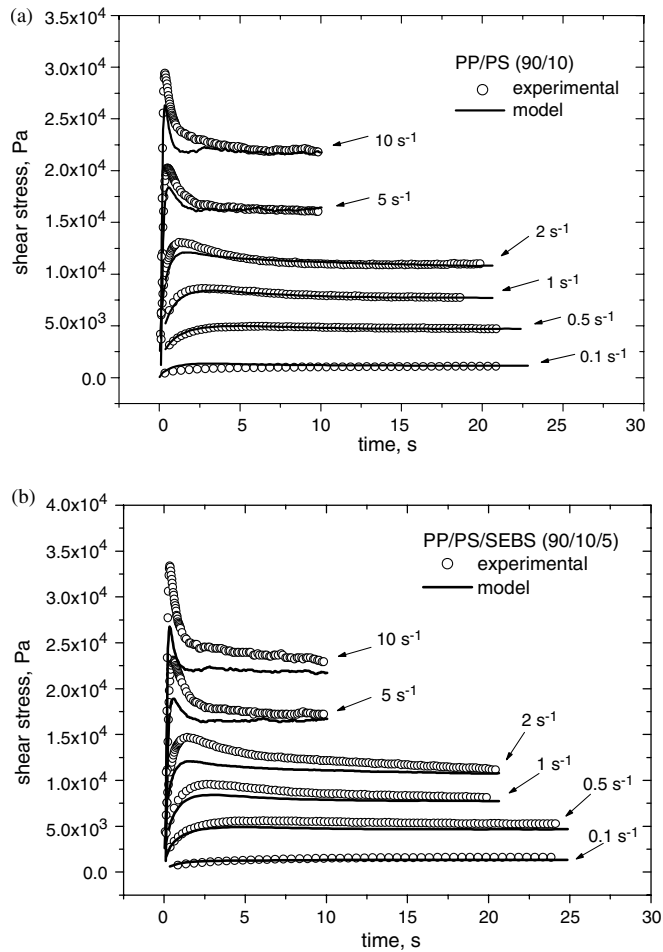
Table 5 Interface contribution to the stress: comparison of model with experiment

Rate (s^{-1})	PP/PS 90/10 $\dfrac{\sigma_{predicted}^{interface}}{\sigma_{experimental}^{interface}}$	PP/PS/SEBS 90/10/5 $\dfrac{\sigma_{predicted}^{interface}}{\sigma_{experimental}^{interface}}$	PP/PS 99/01 $\dfrac{\sigma_{predicted}^{interface}}{\sigma_{experimental}^{interface}}$	PP/PS/SEBS 99/01/10 $\dfrac{\sigma_{predicted}^{interface}}{\sigma_{experimental}^{interface}}$
0.1	0.83	0.63	2.55	1.39
0.5	1.06	0.35	1.63	0.64
1	0.85	0.33	1.21	0.28
2	0.83	0.24	0.62	0.09
5	0.64	0.24	0.37	0.079
10	0.45	0.17	0.16	0.067

Fig. 15.a Experimental and theoretical shear stress for a PP/PS 90/10 blend under single step shear rate. **b** Experimental and theoretical shear stress for a PP/PS/SEBS 90/10/5 blend under single step shear rate
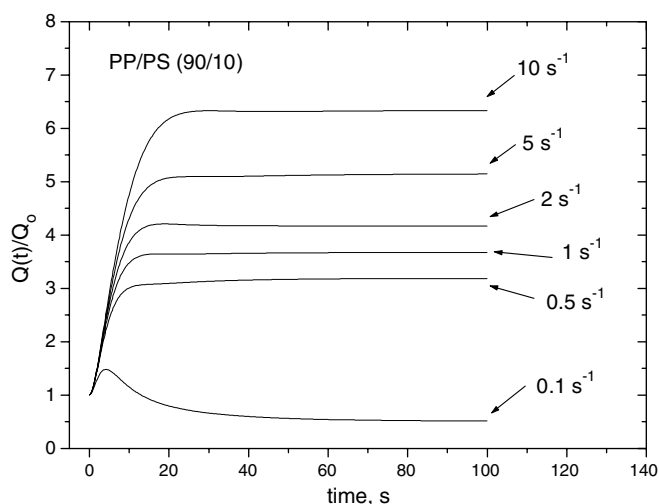
Fig. 16 Prediction of normalized interfacial area per unit of volume for a PP/PS 90/10 blend under single step shear rate
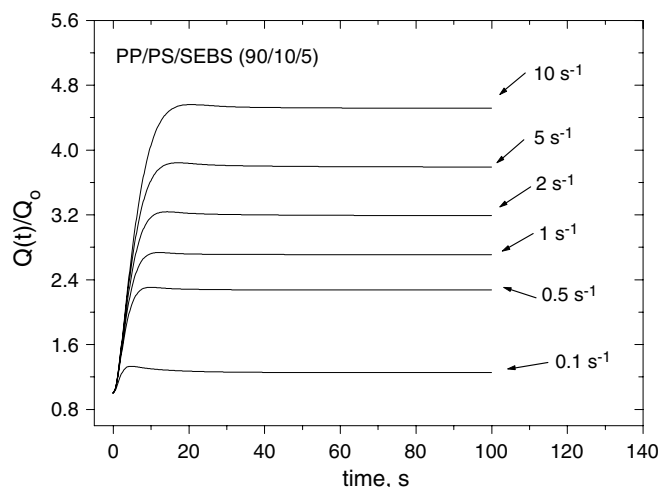

Fig. 17 Prediction of normalized interfacial area per unit of volume for a PP/PS/SEBS 90/10/5 blend under single step shear rate

PP/PS (90/10) and PP/PS/SEBS (90/10/5) blends, respectively. Similar results were obtained for the PP/PS (99/01) and PP/PS/SEBS (99//01/10) blends.

Figure 16 shows that the normalized total surface area per unit volume for the PP/PS blend subjected to a shear rate of 0.1 s^{-1} increases, passes through a maximum, and then levels off at a value smaller than one, indicating that coalescence occurs. At 0.1 s^{-1} the capillary numbers (Ca) of PP/PS (90/10) and (99/01) are 0.24 and 0.06, respectively, therefore, smaller than the critical one ($Ca_{cri} = 0.47$), which exclude droplet break-up. Experimental evidence of coalescence could not be

checked in this work. For shear rates higher than 0.2 s^{-1} for PP/PS blends and for all shear rates for PP/PS/SEBS (Fig. 17) blends the normalized interfacial area per unit volume increases and then levels off at a value greater than one. For shear rates between 0.2 and 10 s^{-1}, the capillary numbers range from 1 to 4.8 for the PP/PS (90/10) blend and from 0.26 to 1.27 for the PP/PS (99/01) blend, indicating that the increase of the normalized total surface area per unit volume is due to deformation and break-up of the dispersed phase.

Figure 18 shows the relation between the phenomenological parameter λ and the shear rate for blend PP/PS (90/10). Similar results were obtained for the other PP/PS and PP/PS/SEBS blends.

The value of λ increases with shear rate, indicating that the interface moves faster when the shear rate increases, and followed the trend in the steady-state total stress (Fig. 9). Also Table 4 shows that λ decreases in the presence of SEBS, most likely due to the enhanced viscosity of PS + SEBS as compared with PS (Macaúbas and Demarquette 2001).

Prediction of the Evolution of Morphology

The modeling of the shear stress in the PP/PS and PP/PS/SEBS blends provides a quantitative description of the morphology evolution as indicated by the total surface area per unit volume ($Q(t)$). The experimental observations of the evolution of morphology (Table 1) were compared to the model predictions.

Samples of PP/PS and PP/PS/SEBS blends subjected to single-step shear were allowed to relax for some time after stopping the shear. Shear rates of 5 and 10 s^{-1} were applied for 10 s, and the relaxed samples were removed
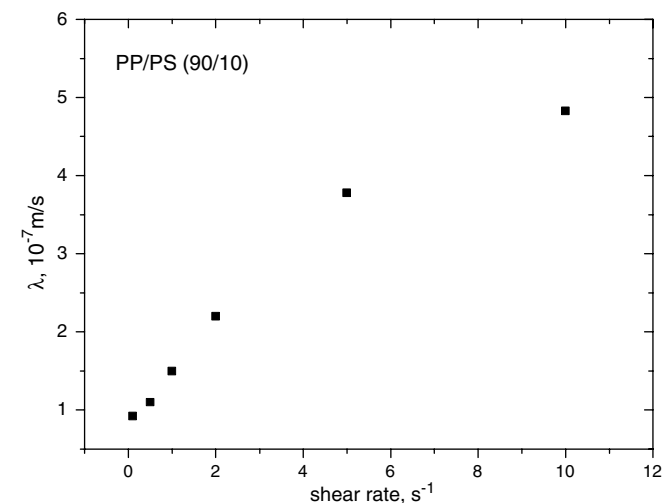

Fig. 18 λ as a function of shear rate for a PP/PS 90/10 blend

from the sliding plate rheometer following the procedure described in the microscopy section. The morphology noted by SEM thus corresponded to a relaxed state rather than the one during flow. In order to predict the evolution of the morphology after cessation of shear, the shear rate was set equal to zero in Eqs. (8) and (9) to give

$$\frac{\partial q_{ij}}{\partial t} = -\lambda Q q_{ij} + \lambda \mu q_{ij}(Q - q) \qquad (22)$$

$$\frac{\partial Q}{\partial t} = -\lambda \mu Q q - \lambda Q d(1 - \mu)q \qquad (23)$$

where

$$q = \sqrt{\sum_{ij} q_{ij}^2} \qquad (10a)$$

with initial conditions: $q_{ij}(0) = q_{ij}(10)$ and $Q(0) = Q(10)$.

The values of the phenomenological parameters were taken to be those found by fitting shear stress data to the model. The resolution of the set of differential equations shown above led to the fact that both q_{ij} and Q tend toward zero at infinite time, indicating that for sufficiently long times the deformed dispersed phase relaxes and approaches a spherical equilibrium with no preferential orientation of the interface and that the total surface area per unit volume does not approach a steady value. Instead, the model predicts phase separation just like a 50/50 blend, in agreement with the Doi-Ohta theory. This is not reasonable for the volume fractions of 1 and 10% used in the present study. Therefore, the interface contribution given by the model of Bousmina et al. (2001) could not be used to predict the morphology after a single-step shear rate.

In order to avoid this singularity two alternative routes were used to model the flow-morphology relationship. 1) It was assumed that the relaxed morphology observed by SEM presents a total surface area per unit volume close to the one just after cessation of shear $Q(10)$, 2) The Doi-Ohta equation relating the steady-state morphology to the flow was used in the form given by Eq. (24):

$$Q(\infty) = \frac{1}{\lambda(1 + \mu)} \sqrt{\frac{1 - \mu}{3\mu}} \dot{\gamma} \qquad (24)$$

Table 6 shows the morphology of the PP/PS and PP/PS/SEBS blends observed after relaxation following single-step shear rate tests, as obtained from scanning electron micrographs (SEM) along with the ones calculated using the two methods described above. We see that there is no agreement between the predicted and experimental morphologies for any blend or shear rate.

Table 6 Volume-averaged radius of droplets: data and model predictions

Material	Rate (s^{-1})	Microscopy R_v(µm)	Q(10) R_v(µm)	Eq. 24 R_v(µm)
PP/PS	5	1.31	0.33	0.15
90/10	10	1.24	0.30	0.13
PP/PS/SEBS	5	0.68	0.19	0.20
90/10/5	10	0.68	0.17	0.11
PP/PS	5	0.34	0.070	0.25
99/01	10	0.34	0.066	0.19
PP/PS/SEBS	5	0.22	0.050	0.20
99/01/10	10	0.22	0.048	0.17

The lack of agreement between experimental and predicted values of volume average radius (R_v) suggests that although the modeling qualitatively describes well the nonlinear rheological behavior of PP/PS blends it seems to underestimate the interface contribution, as shown in Table 5, especially for higher shear rates. In fact, the interface tensor q_{ij} and the total surface area per unit volume (Q) in Doi and Ohta (1991) theory provide an average representation of orientation and size of the deformed dispersed phase, also, no information on the dispersed phase is considered, i.e. the model has no length scale. New terms seem to be necessary to describe the interface contribution quantitatively. Also, relaxation of deformed interfaces is not completely well described. In the case of PP/PS/SEBS blends these issues are even more important due to the presence of a compatibilizer that modifies the interface and requires more complex boundary conditions for modeling.

Double and multi-step shear rates

The same analysis of modeling and morphology evolution were applied to double- and multi-step shear rate tests. For the double-step shear rate tests the initial conditions for the second step shear rate $q_{ij}(0)^{second}$ were taken to be those of $q_{ij}(10)$ and $Q(10)$, i.e., the final state of the interface tensor and the total surface area per unit volume for a single step shear rate test. For the multi-step shear rate tests, the same procedure was used for the subsequent shear rate steps. It was observed that following these procedure the profile of the interface tensor component $q_{12}(t)$ was never the expected one involving an overshoot (when increasing the shear rate) or an undershoot (when decreasing the shear rate), followed by a steady state, even though the phenomenological parameters were adjusted to arrive at such a prediction. Therefore, it was not possible to model the shear stress behavior and correlate it to the morphology evolution for double and multi-step shear rate tests. This failure may be related to the absence of a length scale in the Doi-Ohta theory.

Conclusions

The nonlinear viscoelastic behaviors of PP/PS and PP/PS/SEBS blends having a dispersed droplet morphology were studied by measuring their responses to single, double and a multi-step shear rate tests. The morphology of the samples was determined before and after shearing. The following conclusions can be drawn.

Evolution of morphology

The type of morphology is not changed by shearing, and the average diameter of the dispersed phase decreases for all flow histories when the blend is not compatibilized. When the blend is compatibilized, the average diameter of the dispersed phase changes only for the stronger strain histories.

Single step shear rate

1. There is a shear stress overshoot during the first stages of flow followed by a steady state, showing that for the flow conditions studied the viscoelastic behavior of the blend is nonlinear. The first normal stress difference increases monotonically and approaches a steady-state value.
2. The overshoot and steady-state stresses increase with the addition of SEBS as a result of modification of the interface by this compatibilizer, whereas the time at which the stress overshoot occurs is not affected by the presence of compatibilizer.
3. For all blends, the time of the stress overshoot is inversely proportional to the shear rate, indicating that the orientation of the dispersed phase occurs at a fixed value of the strain.
4. Neither the steady stress nor the interface contribution to the total stress scale linearly with shear rate. The first normal shear stress difference scales linearly with the shear rate.

Double and multi-step shear rates

1. When applying double-step shear rates, a stress overshoot was observed when the shear rate was increased from 5 to 10 s^{-1}, and stress undershoot was observed when the shear rate was decreased from 10 to 5 s^{-1} or reversed from 10 to −10 s^{-1}. For multi-step shear rates, overshoots and undershoots were observed when the shear rate was changed, going from the third step (−10 s^{-1}) to the fourth (5 s^{-1}), and from the fourth (5 s^{-1}) to the fifth (−5 s^{-1}).
2. For all shear histories (increasing, decreasing or reversing) the overshoot stress corresponding to the second step shear rate is below the value obtained for a single-step shear rate. The time at which the stress over/undershoot occurs decreases when the shear rate either increases or decreases if the shear direction is unchanged, but the time at which stress undershoot occurs increases when the direction of the flow is reversed. These variations in the overshoot/undershoot stresses and the time at which they occur could not be attributed solely to the rheological behavior of the individual phases, and are probably due to the evolution of the morphology, e.g., further orientation or a more complex evolution in the case of a reversing flow.

Modeling

1. The theoretical predictions agreed reasonably well with the behavior of the uncompatibilized blends for single-step shear rates, although larger deviations were observed as the shear rate increased and in the determination of the stress overshoot/undershoots. The models considered in this work were not able to predict the stress behavior of PP/PS/SEBS blends, even at small concentration of SEBS due to the absence of the contribution of compatibilizers.
2. It was not possible to model the behavior of the shear stress for double-step shear experiments due to the singularity of the initial conditions.
3. The prediction of the evolution of morphology did not corroborate the experimental results.

References

Almusallam AS, Larson RG, Solomon MJ (2000) A constitutive model for the prediction of ellipsoidal droplet shapes and stresses in immiscible blends. J Rheol 44:1055–1083

Batchelor GK (1970) The stress system in a suspension of force-free particles. J Fluid Mech 41:545–570

Bousmina M, Aouina M, Chaudhry B, Guénette R, Bretas RES (2001) Rheology of polymers blends: non-linear model for viscoelastic emulsions undergoing high deformation flows. Rheol Acta 40:538–551

de Bruijin RA (1989) Deformation and breakup of drops in simple shear flows. PhD thesis, Edinhoven University of Technology, Edinhoven, The Netherlands

Dealy JM, Soong SS (1984) A parallel plate melt rheometer incorporating a shear stress transducer. J Rheol 28:355–365

Demarquette NR, Dealy JM (1992) Nonlinear viscoelasticity of concentrated polystyrene solutions: sliding plate rheometer studies. J Rheol 36:1007–1032

Doi M, Ohta T (1991) Dynamics and rheology of complex interfaces. I. J Chem Phys 95:1242–1248

Giacomin AJ, Samurkas T, Dealy JM (1989) A novel sliding plate rheometer for molten plastics. Polym Eng Sci 29:499–504

Grmela M, Bousmina M, Palierne JF (2001) On the rheology of immiscible blends. Rheol Acta 40:560–569

Guenther GK, Baird DG (1996) An evaluation of the Doi-Ohta theory for an immiscible polymer blend. J Rheol 40:1–20

Hayashi R, Takahashi M, Kajihara T, Yamane H (2001) Application of large double-step shear strain to analyze deformation and shape recovery of a polymer droplet in an immiscible polymer matrix. J Rheol 45:627–639

Iza M, Bousmina M, Jérôme R (2001) Rheology of compatibilizad immiscible viscoelastic polymer blends. Rheol Acta 40:10–22

Jackson NE, Tucker CL (2003) A model for large deformation of an ellipsoidal droplet with interfacial tension. J Rheol 47:659–682

Jeon HK, Macosko C (2003) Visualization of block copolymer distribution on a sheared drop. Polymer 44:5381–5386

Lacroix C, Grmela M, Carreau PJ (1998) Relationship between rheology and morphology for immiscible molten blends of polypropylene and ethylene copolymers under shear flow. J Rheol 42:41–62

Lacroix C, Grmela M, Carreau PJ (1999) Morphological evolution of immiscible polymer blends in simple shear and elongational flows. J Non-Newtonian Fluid Mech 86:37-59

Lee HM, Park OO (1994) Rheology and dynamics of immiscible polymers blends. J Rheol 38:1405–1425

Macaúbas PHP (1999) Determinação da tensão interfacial entre materiais poliméricos através de medidas reológicas. Master dissertation, Escola Politécnica da Universidade de São Paulo, Brasil

Macaúbas PHP, Demarquette NR (2001) Morphologies and interfacial tensions of immiscible polypropylene/polystyrene blends modified with triblock copolymers. Polymer 42:2543–2554

Maffetone PL, Minale M (1998) Equation of change for ellipsoidal drops in viscous flow. J Non-Newtonian Fluid Mech 78:227–241

Onuki A (1987) Viscosity enhancement by domains in phase-separating fluids near the critical point: proposal of critical rheology. Phys Rev A 35:5149–5155

Osaki K, Ohta S, Fukuda M, Kurata M (1976) Nonlinear viscoelasticity of polystyrene solutions. III. Stress development at the start of steady shear flow and an experimental check of some constitutive models. J Polym Sci Polym Phys Ed 14:1701–1715

Takahashi Y, Kurashima N, Noda I, Doi M (1994a) Experimental tests of the scaling relation for textured materials in mixtures of two immiscible fluids. J Rheol 38:699–712

Takahashi Y, Kitade S, Kurashima N, Noda I (1994b) Viscoelastic properties of immiscible polymer blends under steady and transient shear flows. Polym J 26:1206–1212

Underwood EE (1970) Quantitative stereology. Addison Wesley, Reading MA

Velankar S, Puyvelde PV, Mewis J, Moldenaers P (2001) Effect of compatibilization on the breakup of polymeric drops in shear flow. J Rheol 45:1007–1019

Velankar S, Puyvelde PV, Mewis J, Moldenaers P (2004) Steady-shear rheological properties of model compatibilized blends. J Rheol 48:725–744

Vinckier I, Moldenaers P, Mewis J (1996) Relationship between rheology and morphology of model lends in steady shear flow. J Rheol 40:613–631

Yu W, Bousmina M (2003) Ellipsoidal model for droplet deformation in emulsions. J Rheol 47:1011–1039

Yu W, Bousmina M, Grmela M, Palierne JF, Zhou C (2002) Quantitative relationship between rheology and morphology in emulsions. J Rheol 46:1381–1399